Molecular configurations in the droplet detachment process of a complex liquid

R. Sattler,[1] A. Kityk,[1,2,3] and C. Wagner[1,*]
[1]*Experimentalphysik, Universität des Saarlandes, Postfach 151150, 66041 Saarbrücken, Germany*
[2]*Institute for Computer Science, Technical University of Czestochowa, Armii Krajowej 17, PL 42-200 Czestochowa, Poland*
[3]*Institute of Physical Optics, Dragomanova Street 23, Lviv, Ukraine*
(Received 9 November 2006; published 31 May 2007)

We studied the microscopic polymer conformations in the droplet detachment process of an elastic semidilute polyelectrolytic xanthan solution by measuring the instantaneous birefringence. As in earlier studies, we observe the suppression of the finite time singularity of the pinch-off process and the occurrence of an elastic filament. Our microscopic measurements reveal that the relatively stiff xanthan molecules are already significantly prestretched to about 90% of their final extension at the moment the filament appears. At later stages of the detachment process, we find evidence of a concentration enhancement due to the elongational flow.

DOI: 10.1103/PhysRevE.75.051805 PACS number(s): 83.80.Rs, 47.55.D−, 47.20.Gv, 47.20.Dr

I. INTRODUCTION

The addition of a tiny amount of polymer to a simple liquid alters the dynamics of the droplet detachment process dramatically. Instead of the finite time singularity of the minimum neck diameter [1], a cylindrical filament is formed and the shrinking dynamics can be slowed down by several decades [2–5]. Despite the technological relevance of the droplet-forming process of complex liquids, which reaches from plotting of DNA microarrays to food processing, only little is known about the underlying physical mechanisms. In addition to the complexity of the problem and the lack of a universally applicable constitutive equation for complex liquids, there exist no microscopic data about the molecular conformation in such a flow. It is the goal of this study to close this gap.

Earlier experimental studies on the droplet detachment process of complex liquids were limited to the analysis of macroscopic quantities, like the determination of the shape of the thinning filament. These can be compared with theoretical analyses on capillary breakup based on phenomenological polymer models like, e.g., the Oldroyd-B model or models that follow from kinetic theory like the finitely extensible nonlinear elastic Perterin (FENE-P) model [6]. But for a true comparison with microscopic models, the dynamics of the polymers on the molecular level must be measured. Birefringence is a typical tool for such investigations [7], and we use a high-speed setup capable of capturing dynamics on the time scale of milliseconds to study simultaneously both the microscopic conformation and the macroscopic flow response in the elastic thread.

II. SAMPLE CHARACTERIZATION

The polymeric system of our study, xanthan (Sigma-Aldrich), was chosen because of its high optical anisotropy. The molecule is relatively stiff and the formation of an elastic filament is not observed in aqueous solutions [4] but only in experiments with more viscous solvents [5]. We also tried to measure birefringence for more flexible polymers like polyethylenoxide (PEO) or polyacrylamide-co-acrylic acid (PAA), but signals were too low to allow for a quantitative analysis. The molecular weight m of our polymer is vaguely specified by the distributor as $m=2\times10^6$ amu or more. Xanthan shows a pronounced shear thinning and biological digestibility and, for both reasons, it is widely used in the food, pharmaceutical, oil, and cosmetic industries. The ordered molecule exists in solution as a semirigid helix with a persistence length of $\ell_p=120$ nm. It undergoes a conformational transition to a disordered flexible coil only above a temperature of 50 °C [8,9].

Our sample solutions were prepared with weight concentrations c_p in the semidilute regime from $0.025<c_p<0.2$ wt %, mostly dissolved in 80-20 wt % glycerol-water as a solvent with a viscosity of $\eta_{solv}=60$ mPa s. We also used different glycerol-water weight ratios, resulting in solvent viscosities down to $\eta_{solv}=2$ mPa s only to allow for a better determination of the molecular weight of our sample by fitting our extensional rheological data. The polymer concentrations were chosen to obtain a sufficiently high birefringence but still to be significantly below concentrations at which spontaneous lyotropic ordering is expected in equilibrium ($c_p>0.5$ wt %) [8]. Standard rheological measurements, using a cone plate geometry on a standard rheometer (Haake Mars, Thermo Electron, Germany), were performed to characterize the shear thinning behavior (Fig. 1) of our samples. Stationary experiments controlling either shear rate or tension were repeated several times for several samples in a cone plate geometry with an angle of 0.5° and a diameter of 60 mm. Depending on the experimental deviations an average of between six and ten measurements is shown. The solutions show a pronounced shear thinning, as is to be expected for relatively stiff molecules approaching a stationary value slightly enhanced compared to the pure Newtonian solvent according to the polymer concentration. The data have been approximated using the Carreau model [11]and the results are in reasonable agreement with Ref. [10] if one takes our higher solvent viscosities into account. The characteristic relaxation times of the fits range from about 10 s for 0.5 wt % and 20 s for 0.1 wt % to about 50 s for the 0.2 wt % solution. These time scales give a measure for the

*Electronic address: c.wagner@mx.uni-saarland.de

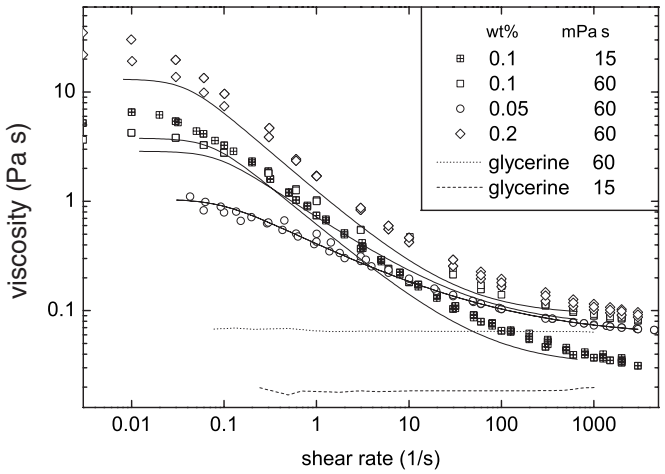

FIG. 1. Stationary viscosities from shear rate and stress controlled measurements. Not all experiments and data points are shown. The lines are approximations by the Carreau model.

rotational diffusion time of our molecules and must be compared with the elongational rates in our droplet experiments.

For the later discussion of our elongational viscosity measurements we would like especially to point out that the 0.1 wt % samples with different solvent viscosities show similar zero shear rate viscosities, and the differences only become obvious at high shear rates.

Finally, the surface tensions σ of our samples were determined with the pending droplet method. Within the experimental resolution of ±5% we could not observe any differences from the tabulated values for glycerol-water mixtures.

III. EXPERIMENTAL SETUP

The experimental setup is sketched in Fig. 2(a). The polymer solutions are quasistatically driven through a nozzle of $d=2$ mm diameter by a syringe pump. At a distance of $D=7$ cm below the nozzle, a plate is mounted in order to omit gravitational effects. The cylindrical filament is formed only after the droplet reaches the bottom plate, and in this way the filament is stabilized against air currents. All measurements have been performed at room temperature (25 °C). The retardation δ is measured using an optical train consisting of an 18 mW HeNe laser (JDS Uniphase), a polarizer (P), a photoelastic modulator (PEM) (Hinds Instruments), the sample liquid, an analyzer (A), a bright-field lens system ($L1$ and $L2$), and a photodiode (PD) connected to two lock-in amplifiers (Stanford Research). The polarizer is fixed at an angle of 45° relative to the photoelastic modulator which allows for a lock-in technique for the detection of the retardation signal. The bright-field lens system [Fig. 2(b)] in front of the detector prevents any light that has not crossed the filament (Fig. 3) from reaching the detector by blocking the parallel components with a mask M in the focal point of lens $L1$. The lens $L2$ collects the light that is diffused by the cylindrical filament into the detector [12]. To calculate the birefringence $\Delta n=\delta\lambda/[2\pi h(t)]$ (with $\lambda=633$ nm as the HeNe laser wavelength) from the retardation signal, the instantaneous thickness $h(t)$ of the filament must be known. The thinning process of the filament diameter $h(t)$ is measured at 500 frames per second with a high-speed charge-coupled device camera (Encore Mac PCI 1000S) that is placed perpendicular to the optical train. The camera is equipped with a 2× magnifica-

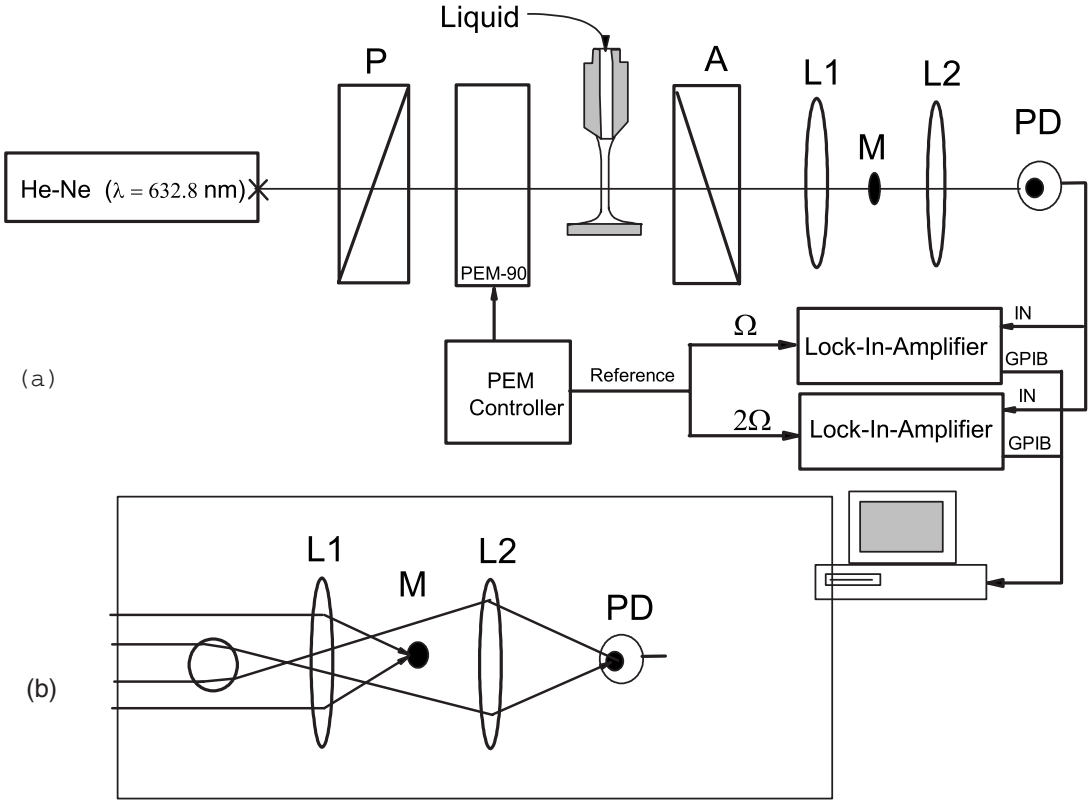

FIG. 2. Experimental setup. See text for further explanation.

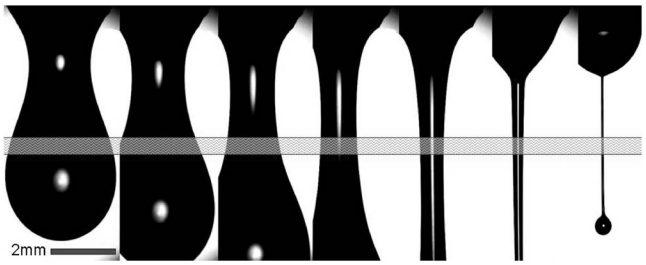

FIG. 3. Photographs of the droplet detachment process of a 0.2 wt % xanthan solution (η_{solv}=60 mPa s) taken every 0.1 s, indicating, schematically, the laser beam positioned close to the neck and in a region as cylindrical as possible throughout the measurement.

tion objective and the image capturing is synchronized to the data collection of the two lock-inamplifiers. From Fig. 3 it becomes obvious that, for geometric reasons, it is impossible to measure birefringence before the droplet has completely passed the light beam and the temporal exponentially thinning filament is present. This is the moment when our measurements start.

IV. EXPERIMENTAL RESULTS

A. Macroscopic measurements

Different regimes can be distinguished in analyzing the temporal behavior of the neck diameter $h(t)$ in the droplet detachment process of a polymer solution. First, it follows an exponential law that is well described by the Rayleigh instability of Newtonian liquids [13,14]. Then it might pass into the self-similar regimes that describe the breakup of Newtonian liquids [15], until the polymers intervene in the flow abruptly and a filament is formed which, again, thins very slowly and exponentially with time [16], until it might reach eventually the state where all polymers are fully stretched and the thinning process becomes linear [17].

Figure 4 shows the filament thickness $h(t)$ extracted from the video images that start at the moment when the filament is formed. More viscous solvents or higher polymer concentrations lead to a slower dynamic that differs by more than an order of magnitude. However, at first all runs show the same exponential thinning behavior, followed by a linear regime, and the data can be approximated by the expression

$$h(t) = h_0 \exp(-t/\tau) - bt + y_0. \tag{1}$$

The formation of the cylindrical filament occurs due to the high resistance of the polymers to elongational flow, and this resistance is macroscopically quantified by the elongational viscosity η_e. The same form of Eq. (1) has been used to fit data from extensional rheology measurements (both capillary breakup and filament stretching devices [17]). Its physical meaning is that first the polymer molecules are uncoiled by the flow and the dynamic is governed purely by elastic effects. Once the polymers are stretched, a steady state is reached which leads to a linear dynamic that might be similar to the linear thinning dynamic near breakup of Newtonian

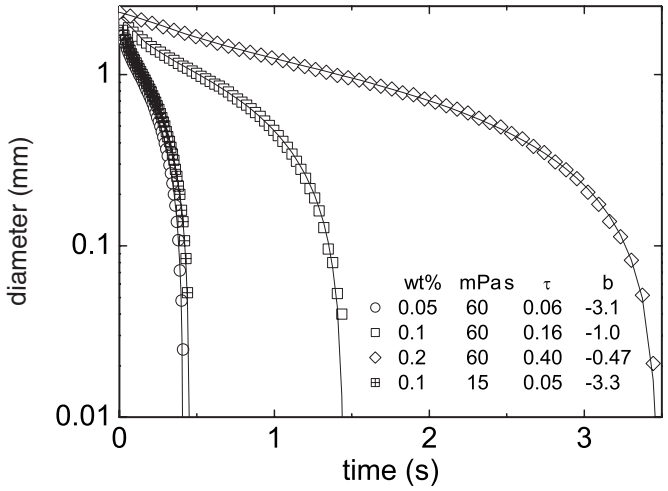

FIG. 4. Filament diameter $h(t)$ for different polymer concentrations and solvent viscosities. The parameters refer to Eq. (1). Not all data points are shown.

liquids [13]. From $h(t)$ one can calculate the corresponding elongational rates $\dot{\epsilon}=\partial_t h(t)/h(t)$. These have to be compared with characteristic relaxation times. The microscopic polymer rotational diffusion has been estimated by the time constants from the standard rheological measurements to be at least $\lambda > 10$ s and the appropriate ratio is given by the Weissenberg number which is always found to be very large, $\mathrm{Wi}=\lambda\dot{\epsilon} > 100$ in our experiments. This means that the polymer molecules in the droplet detachment process do not experience a force field that is comparable to the Brownian forces and time scales, but are affected by a violent flow and stretched and oriented in a deterministic manner. Nevertheless, the elongational rates and the Weissenberg numbers are practically constant in the regime of exponential thinning. They diverge, though, when the linear thinning behavior sets in.

The $h(t)$ data can also be used directly to calculate the apparent elongational viscosity by equating the capillary pressure with the elastic stresses [3,4,17]:

$$\eta_e(t) = \frac{2\sigma}{\dot{\epsilon}h(t)}. \tag{2}$$

This approach is a simplification because it neglects gravitational or nonlinear elastic effects, but it is commonly used to extract the elongational viscosity from capillary break up experiments. A common quantity representing the stress- and stretching history of the fluid, and thereby the polymers, is the Henky strain given by $\zeta=\int \dot{\epsilon}\, dt$. The corresponding elongational viscosity data in Fig. 5 first show an exponential increase of the apparent elongational viscosity followed by a steady state value for strains $\zeta \geq 1.5$. The observation of the plateau value at strains that are much smaller compared to earlier work [4,17,18] is a consequence of the relative stiffness of the xanthan molecule and the prestretching before the occurrence of the filament. This is also indicated by the elevated elongational viscosity at $\zeta=0$. If the filament started to be formed with the polymers at rest, one

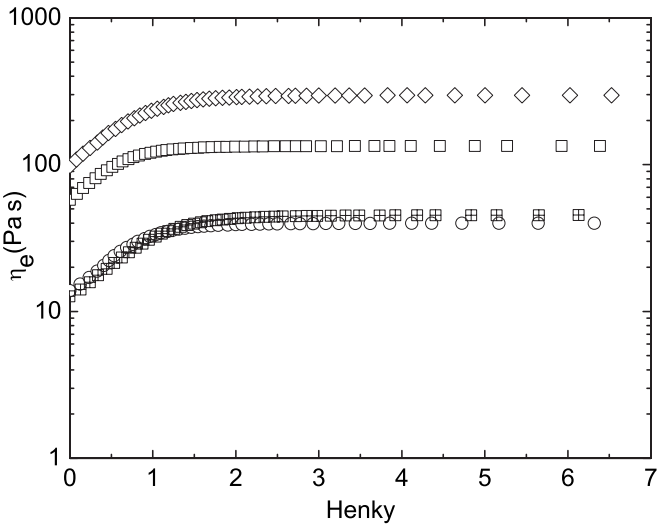

FIG. 5. Apparent elongational viscosity for the same set of data as in Fig. 4.

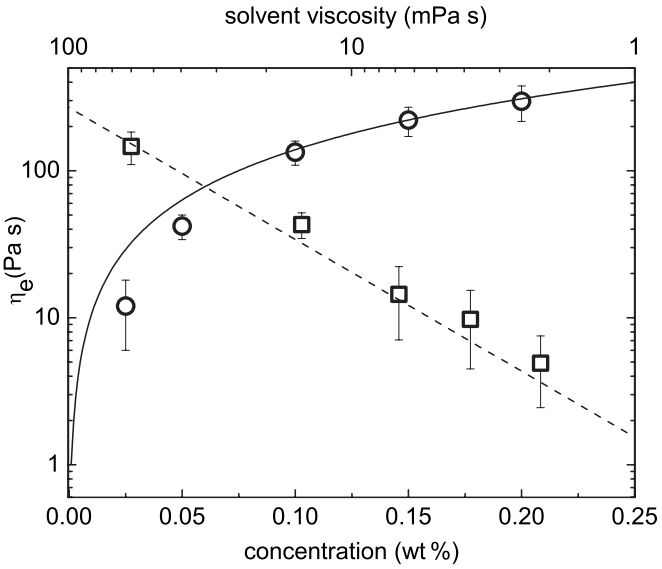

FIG. 6. Elongational viscosity for different solvent viscosities (squares) and polymer concentrations (circles). The data are taken at large Henky strain (compare Fig. 5). The continuous and the dashed lines show the theoretical values according to a fit with Bachelor's formula for semidiluted rigid rods.

would expect the elongational viscosity to grow from the Newtonian value of the so-called Trouton ratio $\eta_e/\eta_s=3$. When η_e reaches the plateau value, the thinning dynamic becomes linear and the elongational rate $\dot{\epsilon}$ diverges, indicating that η_e is independent of the elongational rate, as predicted by rigid rod models as well as elastic models for $Wi \gg 1$ [19]. The measured elongational viscosities are in reasonable agreement with data from studies with opposing nozzles [20], fiber spinning devices [21], or values obtained by analyzing contraction flow [22].

To characterize our sample polymer we needed an estimate for its molecular weight, and we used Batchelor's formula [24] for the elongational viscosity of semidiluted rigid rods to fit our data. Fluorescence microscopy studies on DNA show that at steady state for Henky strains $\zeta \geq 1.5$ the molecules are extended to a maximum hydrodynamic length ℓ that is more than 80% of their contour length [23], and the relatively stiff xanthan molecules are mostly well approximated as rigid rods. In order to allow for a robust fitting procedure for the determination of the two free parameters molecular weight m and polymer length ℓ, we varied both the polymer concentration and the solvent viscosity. As expected we found the elongational viscosity to always be proportional to the solvent viscosity (see Fig. 5). With our two independent sets of data, we performed the fit with Batchelor's formula for semidiluted solutions of rigid rods [24] (Fig. 6),

$$\eta_e = 3\,\eta_{solv} + \frac{\frac{2}{3}\eta_{solv}\Phi(\ell/d)^2}{\ln(2\,\ell/d) - \ln(1 + 2\sqrt{\Phi/\pi}\,\ell/d) - 1.5}. \quad (3)$$

$\Phi=(\pi d^2 \ell N_A c_p)/(4Mw)$ is the particle volume fraction, ρ (g/cm^3) the density of the solvent, N_A is Avogadro's number, and, for the width of the polymer, we took the literature value of $d=2$ nm. The fit yields $\ell=4.5$ μm and $m=2.5$ M amu. This ratio of molecular weight and length is in very good agreement with, e.g., the results from a contraction flow study by [22], but differs by a factor of 2 from values obtained by light scattering [20]. The number of Kuhn steps $n_k=\frac{1}{2}\ell/\ell_p$ of our sample is about 40, a value that is ten times smaller than that of λ-DNA, which was used in a previous study where no steady state of the elongational viscosity had been observed [18].

B. Birefringence measurements

We can now turn to the microscopic study of the conformation of the macromolecules by means of the birefringence measurements. An elaborate introduction to optical flow rheometry is given in [7]. In our unidirectional stretching geometry with the flow along the direction of gravity, we can assume transverse isotropy for polarizability and segmental order of the single units of the macromolecules. Therefore, the birefringence signal ΔN is proportional to the segmental order of the polymers and to their concentration,

$$\Delta N = \frac{2\pi}{nm}\Delta\alpha_0 c_p \rho \frac{1}{2}\langle 3\cos^2\theta - 1\rangle \quad (4)$$

where n is the average refractive index, $\Delta\alpha_0$ the anisotropy of polarizibility per molecule of a complete stretched chain, and θ the orientation angle of the polymer segments to the direction of extension. By knowledge of the maximum birefringence signal ΔN_{max} at maximum extension and alignment of the polymers, the mean fractional extension of our polymers is then $x/\ell=\sqrt{(2\Delta N/\Delta N_{max}+1)/3}$, because, on a microscopic scale, a variety of different configurations will certainly be present [23].

The neglect of different configuration types like, e.g., the dumbbell or hairpin, leads to a certain overestimate of the fractional extension, and our calculation loses its accuracy for coiled states. The correctness of the formula improves,

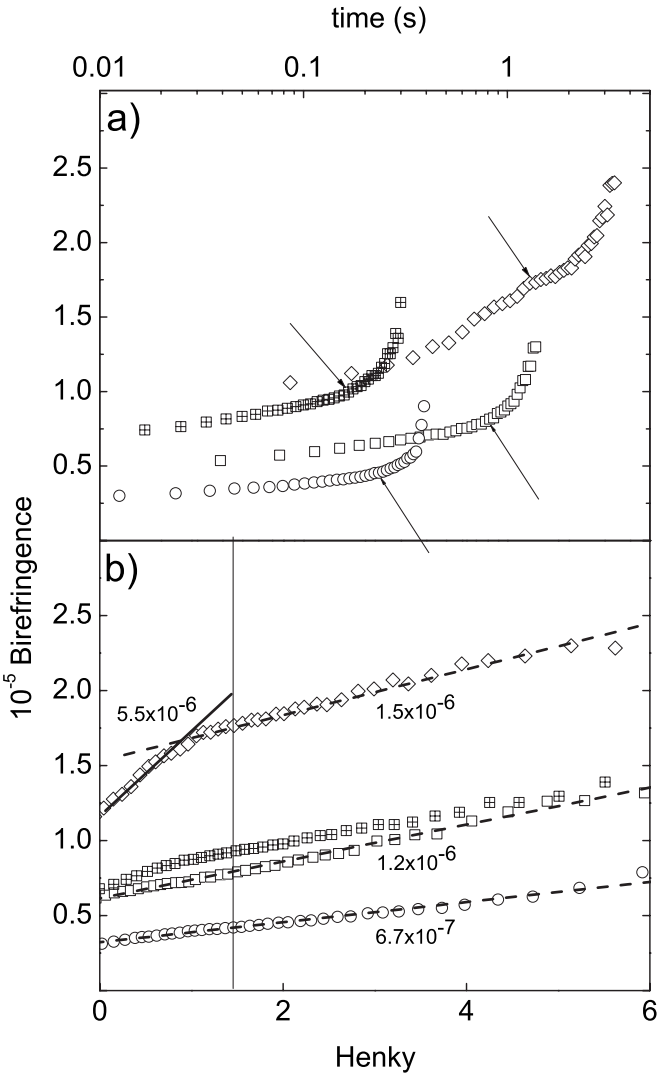

FIG. 7. (a) Instantaneous birefringence versus the elapsed time. The arrows indicate a Henky strain of $\zeta=1.5$. (b) Instantaneous birefringence versus the Henky strain. The vertical line indicates the $\zeta=1.5$ position; the dashed lines are linear fits with slopes indicated by the numbers. Symbols are as in Fig. 1.

though, with increasing degree of orientational order, and it is a good approximation for large fractional extensions of the stretched polymers.

To test the reliability of our method we performed several runs at different polymer concentrations, and the birefringence signal was always roughly proportional to the concentration [Fig. 7(b)]. The robustness and selectivity of our method become clear if one compares the data of the solution with 0.05 wt % of polymer and $\eta_{solvent}=60$ mPa s with the solution with 0.1 wt % of polymer and $\eta_{solvent}=15$ mPa s. Both data sets practically lead to the same flow (Fig. 4) but, exceeding the capabilities of simple extensional rheometry, the birefringence signal is sensitive to the differences in concentration. This shows how important the microscopic measurements are if one wants to qualify theoretical predictions that are based on kinetic models.

The measurements of the birefringence in our setup are restricted to the time t_c after the filament is formed because optical aberrations make it impossible to measure it at earlier stages of the pinching process. Even if the origin of the Henky strain is not influenced much by this limitation, as most of the strain is accumulated at the final stages of the experiment, our data reveal that the polymers have a significant (flow and strain) history when our measurements start. Assuming that the polymers are completely stretched when elastic effects are no longer observable for $\zeta \geq 1.5$, we can determine the maximum birefringence per polymer concentration from our birefringence data $\Delta N_{max}/c_p=\Delta N(\zeta=1.5)/c_p=8\times10^{-2}$ g^{-1} cm^3. This is comparable to the value for fully elongated λ DNA of $\Delta N_{max}/c_p=5.1\times10^{-2}$ g^{-1} cm^3 [25], but a decade larger than values obtained for xanthan in shear flow [26] and in transient electric birefringence measurements [27].

The experimentally measured corresponding maximum birefringence of the $c_p \leq 0.1$ wt % solutions is only 30% larger than at $\zeta=0$. This would correspond to a fractional polymer extension $x/\ell=0.9$ at $\zeta=0$, indicating that stiff polymers like xanthan are almost completely aligned and stretched when the filament occurs. The uncoiling process in the range $0<\zeta<1.5$ correlates with an elastic, exponential filament thinning dynamic and a monotonic increase of the birefringence signal.

However, instead of a plateau value at the final stage of the experiment, we observe a divergence in the birefringence signal [Fig. 7(a)]. The divergence is very reproducible and takes place at stages of the filament thinning process when the filament diameter is still large enough to render the analysis unambiguous. The divergence of the birefringence signal comes along with a divergence in the elongational rate $\dot{\epsilon}$ that follows from the linear shrinking of the filament. Surprisingly, we find that the birefringence signal continues to increase with constant slope from $\zeta=1.5$ to 6 if plotted against the strain. Only for the $c_p \geq 0.15$ wt % solutions did we observe a steeper slope in the birefringence signal for $\zeta<1.5$, presumably because of the stronger entanglement of the polymers.

While the polymers should be completely uncoiled in the linear thinning regime, additional physical mechanisms, that we will discuss in the following, have to be considered. We do see three different possible scenarios. First, there is an effect of the polydispersity of the molecular weight distribution of our sample. But the observed large Wi should lead to a complete stretching of smaller molecules at even smaller strains. Second, there is an overstretching of the molecule by the strong flow that would affect the configurations of the molecular bonds. But this would most presumably also imply an increase in elongational viscosity. Third, there is a concentration enhancement by drainage or evaporation of the solvent. This picture is supported by the observation that, eventually, the filament might not break at the final stages of the thinning process but leave a very thin polymer (<10 μm) fiber between the nozzle and the ground plate. Then a configuration called beads on a string occurs via an instability of the surface of the cylindrical filament [28].

V. CONCLUSION

In conclusion, we have presented the first measurements on the molecular configurations of semirigid xanthan molecules in the droplet detachment process of a complex liquid. We find that stiff molecules like xanthan are highly oriented and stretched by the flow, even before the abrupt transition from the Newtonian self-similar shrinking law to the exponential behavior of the elastic filament. Furthermore, we do observe a further increase of the birefringence signal after the saturation of elastic effects and the stretching of the polymers. We discussed different possible reasons for this phenomenon and find that a concentration enhancement is most likely to be the pertinent effect, but we cannot completely exclude the possibility that changes in the intramolecular bond configurations caused by the violent flow, or effects resulting from polydispersity, affect the birefringence signal too.

[1] For a review, see J. Eggers, Rev. Mod. Phys. **69**, 865 (1997).
[2] M. Goldin, J. Yerushalmi, R. Pfeffer, and R. Shinnar, J. Fluid Mech. **38**, 689 (1969).
[3] A. V. Bazilevskii, V. M. Entov, and A. N. Rozhkov, Sov. Phys. Dokl. **26**, 333 (1981).
[4] Y. Amarouchene, D. Bonn, J. Meunier, and H. Kellay, Phys. Rev. Lett. **86**, 3558 (2001).
[5] L. B. Smolka and A. Belmonte, J. Non-Newtonian Fluid Mech. **137**, 103 (2006).
[6] J. Li and M. A. Fontelos, Phys. Fluids **15**, 922 (2003).
[7] G. G. Fuller, *Optical Rheometry of Complex Fluids* (Oxford University Press, Oxford, 1995).
[8] G. H. Koenderink, S. Sacanna, D. G. A. L. Aarts, and A. P. Philipse, Phys. Rev. E **69**, 021804 (2004), and references therein.
[9] G. Holzwarth and E. B. Prestridge, Science **197**, 758 (1977); W. E. Rochefort and S. Middleman, J. Rheol. **31**, 337 (1987).
[10] F. V. Lopez, L. Pauchard, M. Rosen, and M. Rabaud, J. Non-Newtonian Fluid Mech. **103**, 123 (2002).
[11] R. I. Tanner, *Engineering Rheology* (Oxford Science, Oxford, 1985).
[12] W. H. Talbot and J. D. Goddard, Rheol. Acta **18**, 505 (1979).
[13] A. Rothert, R. Richter, and I. Rehberg, Phys. Rev. Lett. **87**, 084501 (2001).
[14] C. Wagner, Y. Amarouchene, Daniel Bonn, and J. Eggers, Phys. Rev. Lett. **95**, 164504 (2005).
[15] J. Eggers, Phys. Rev. Lett. **71**, 3458 (1993).
[16] V. M. Entov and A. L. Yarin, Fluid Dyn. **19**, 21 (1984).
[17] S. L. Anna and G. H. McKinley, J. Rheol. **45**, 115 (2000).
[18] C. Wagner, P. Doyle, Y. Amarouchene, and D. Bonn, Europhys. Lett. **64**, 823 (2003).
[19] R. B. Bird, C. F. Curtiss, R. C. Armstrong, and O. Hassager, *Dynamics of Polymeric Liquids* (J. Wiley, New York, 1987).
[20] G. G. Fuller, C. A. Cathey, B. Hubbard, and B. E. Zebrowski, J. Rheol. **31**, 235 (1987).
[21] M. Khagram, R. K. Gupta, and T. Sridhar, J. Rheol. **29**, 191 (1985).
[22] A. Mongruel and B. Cloitre, J. Non-Newtonian Fluid Mech. **110**, 27 (2002).
[23] T. T. Perkins, D. E. Smith, and S. Chu, Science **276**, 2016 (1997). D. E. Smith and S. Chu, *ibid.* **281**, 1335 (1998).
[24] G. K. Bachelor, J. Fluid Mech. **46**, 813 (1971).
[25] G. Maret and G. Weill, Biopolymers **22**, 2727 (1983).
[26] N. P. Yevlamppieva, G. M. Pavlov, and E. I. Rjumtsev, Int. J. Biol. Macromol. **26**, 295 (1999).
[27] V. J. Morris, K. Anson, and C. Turner, Int. J. Biol. Macromol. **4**, 362 (1982).
[28] M. S. N. Oliveira and G. H. McKinley, Phys. Fluids **17**, 071704 (2005).